
Since January 2020 Elsevier has created a COVID-19 resource centre with free information in English and Mandarin on the novel coronavirus COVID-19. The COVID-19 resource centre is hosted on Elsevier Connect, the company's public news and information website.

Science of the Total Environment 825 (2022) 153902

Contents lists available at ScienceDirect

Science of the Total Environment

journal homepage: www.elsevier.com/locate/scitotenv

# Bioactive hybrid metal-organic framework (MOF)-based nanosensors for optical detection of recombinant SARS-CoV-2 spike antigen

Navid Rabiee [a,b,*], Yousef Fatahi [c,d], Sepideh Ahmadi [e,f], Nikzad Abbariki [g], Amirhossein Ojaghi [g], Mohammad Rabiee [h], Fatemeh Radmanesh [i], Rassoul Dinarvand [c,d], Mojtaba Bagherzadeh [g], Ebrahim Mostafavi [j,k], Milad Ashrafizadeh [l,m], Pooyan Makvandi [n,**], Eder C. Lima [o,**], Mohammad Reza Saeb [p]

[a] Department of Physics, Sharif University of Technology, P.O. Box 11155-9161, Tehran, Iran
[b] School of Engineering, Macquarie University, Sydney, New South Wales 2109, Australia
[c] Department of Pharmaceutical Nanotechnology, Faculty of Pharmacy, Tehran University of Medical Sciences, Tehran, Iran
[d] Nanotechnology Research Centre, Faculty of Pharmacy, Tehran University of Medical Sciences, Tehran, Iran
[e] Student Research Committee, Department of Medical Biotechnology, School of Advanced Technologies in Medicine, Shahid Beheshti University of Medical Sciences, Tehran 19857-17443, Iran
[f] Cellular and Molecular Biology Research Center, Shahid Beheshti University of Medical Sciences, Tehran 19857-17443, Iran
[g] Department of Chemistry, Sharif University of Technology, Tehran, Iran
[h] Biomaterial Group, Department of Biomedical Engineering, Amirkabir University of Technology, Tehran, Iran
[i] Uro-Oncology Research Center, Tehran University of Medical Sciences, Tehran 14197-33141, Iran
[j] Stanford Cardiovascular Institute, Stanford University School of Medicine, Stanford, CA 94305, USA
[k] Department of Medicine, Stanford University School of Medicine, Stanford, CA 94305, USA
[l] Faculty of Engineering and Natural Sciences, Sabanci University, Orta Mahalle, Üniversite Caddesi No. 27, Orhanlı, Tuzla, Istanbul 34956, Turkey
[m] Sabanci University Nanotechnology Research and Application Center (SUNUM), Tuzla, Istanbul 34956, Turkey
[n] Istituto Italiano di Tecnologia, Centre for Materials Interfaces, viale Rinaldo Piaggio 34, 56025 Pontedera, Pisa, Italy
[o] Institute of Chemistry, Federal University of Rio Grande do Sul (UFRGS), Av. Bento Goncalves 9500, Postal Box, 15003, 91501-970, Brazil
[p] Department of Polymer Technology, Faculty of Chemistry, Gdańsk University of Technology, G. Narutowicza 11, 12 80-233 Gdańsk, Poland

## HIGHLIGHTS

- One-pot synthesis of MOF-5/CoNi2S4 in assistance of high-gravity
- Turning a toxic cobalt-nickel-based nanoparticle into a non-toxic form
- Highly sensitive recombinant SARS-CoV-2 spike antigen optical biosensor

## GRAPHICAL ABSTRACT

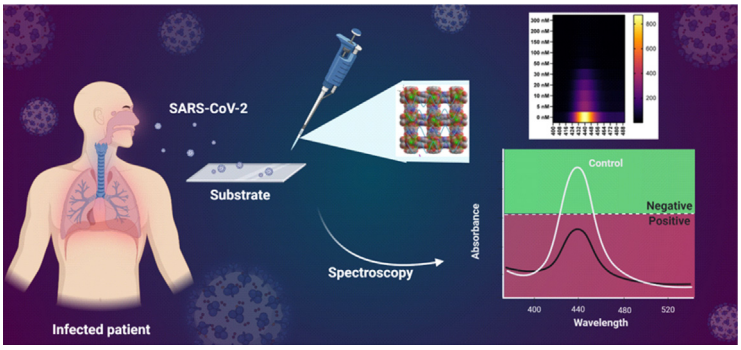


* Correspondence to: N. Rabiee, Department of Physics, Sharif University of Technology, P.O. Box 11155-9161, Tehran, Iran.
** Corresponding authors.
*E-mail addresses:* navid.rabiee@mq.edu.au (N. Rabiee), pooyan.makvandi@iit.it (P. Makvandi), eder.lima@ufrgs.br (E.C. Lima).

http://dx.doi.org/10.1016/j.scitotenv.2022.153902

ARTICLE INFO

*Article history:*
Received 11 January 2022
Received in revised form 7 February 2022
Accepted 11 February 2022
Available online 17 February 2022

Editor: Warish Ahmed

*Keywords:*
COVID-19
MOF-5
High-gravity technique
Recombinant SARS-CoV-2 spike antigen
Biosensor

ABSTRACT

Fast, efficient, and accurate detection of SARS-CoV-2 spike antigen is pivotal to control the spread and reduce the mortality of COVID-19. Nevertheless, the sensitivity of available nanobiosensors to detect recombinant SARS-CoV-2 spike antigen seems insufficient. As a proof-of-concept, MOF-5/$CoNi_2S_4$ is developed as a low-cost, safe, and bioactive hybrid nanostructure via the one-pot high-gravity protocol. Then, the porphyrin, $H_2TMP$, was attached to the surface of the synthesized nanomaterial to increase the porosity for efficient detection of recombinant SARS-CoV-2 spike antigen. AFM results approved roughness in different ranges, including 0.54 to 0.74 μm and 0.78 to ≈0.80 μm, showing good physical interactions with the recombinant SARS-CoV-2 spike antigen. MTT assay was performed and compared to the conventional synthesis methods, including hydrothermal, solvothermal, and microwave-assisted methods. The synthesized nanodevices demonstrated above 88% relative cell viability after 24 h and even 48 h of treatment. Besides, the ability of the synthesized nanomaterials to detect the recombinant SARS-CoV-2 spike antigen was investigated, with a detection limit of 5 nM. The in-situ synthesized nanoplatforms exhibited low cytotoxicity, high biocompatibility, and appropriate tunability. The fabricated nanosystems seem promising for future surveys as potential platforms to be integrated into biosensors.

## 1. Introduction

The coronavirus disease 2019 (COVID-19) is caused by a novel coronavirus (SARS-CoV-2), and it is now one of the major problems of public health worldwide (Drobysh et al., 2022; Drobysh et al., 2021; Dronina et al., 2021; Plikusiene et al., 2021; Yüce et al., 2021). The outbreak of SARS-CoV-2 started in China and spread to other countries of the world, leading to high death in the population (Maddali et al., 2021). It is a positive sense and enveloped RNA beta virus, and the primary target of this virus is the lung. There are some symptoms of SARS-CoV-2, such as fever, cough, fatigue, dyspnea, and anosmia, among others (Hornuss et al., 2020). However, based on estimates, 20% of patients are asymptomatic (Buitrago-Garcia et al., 2020). Furthermore, from time to time, mutation of COVID-19, leading to the advance and spread of Delta and Omicron variants, has become another nightmare, which necessitates quick and very accurate detection of the SARS-CoV-2 spike antigen (Bhavya et al., 2022; Takashita et al., 2022).

Radiography or computed tomography (CT) imaging can be employed to diagnose SARS-CoV-2. Based on the findings, posterior lung areas are commonly involved, and inflammation can be observed. Cavitation, nodules, pleural effusions, and fibrosis are uncommon but can occur (Chung et al., 2020). In laboratory tests, leucopenia, lymphopenia, and hypoalbuminemia are observed (Chen et al., 2020; Huang et al., 2020). After infection, fever is the most common symptom for up to 12 days, and other symptoms such as cough and dyspnea can be developed in the following stages (Zhou et al., 2020). As high numbers of deaths occur worldwide due to the spread of SARS-CoV-2, most of the experiments have focused on developing novel methods for detecting SARS-CoV-2 infection. Various kinds of strategies have been developed to diagnose SARS-CoV-2, including RT-PCR, antibody-based detection methods, antigen-based methods, and CRISPR/Cas9 system, among others (Yüce et al., 2021). However, there are some drawbacks associated with the aforementioned tests. For instance, false results can occur in RT-PCR (Kumar et al., 2022; Shetti et al., 2021; Suleman et al., 2021; Yüce et al., 2021). Recently, studies have designed nanoplatforms for the diagnosis of SARS-CoV-2 in patients. The nanosystems can provide a rapid, reliable, and cost-effective diagnosis of SARS-CoV-2 in patients. To date, various kinds of nanomaterials such as gold nanoparticles, graphene, and iron oxide nanoparticles, as well as lanthanide-doped polystyrene nanostructures, have been designed for SARS-CoV-2 diagnosis (Bidram et al., 2021; Iravani, 2020; Srivastava et al., 2021; Xi et al., 2020).

Metal-organic frameworks (MOFs) are warmly welcomed because their exceptional porous and multifunctional character makes a promising platform extensively applied in medicine as biosensors (Bhardwaj et al., 2017). MOFs have a crystalline structure with a surface potent to functionalization and tunable porosity (Xian et al., 2021). The network of MOFs can be extended by coordinated bonds between the inorganic nodes and organic linkers (Furukawa et al., 2013). MOFs demonstrate high surface area, and because of their biocompatibility and high stability, they are utilized for cargo delivery, bioimaging, and sensing (Quijia et al., 2021). Recently, an experimentalist team developed nickel-MOF and then combined it with Au nanoparticles and carbon nanotubes. The resulting nanostructure can detect HIV based on DNA hybridization (Lu et al., 2021). In another effort, 2D MOF nanoenzymes were designed for electrochemical detection of *Staphylococcus aureus* (Hu et al., 2021). The resulting MOFs demonstrated high peroxidase-like activity and effectively revealed bacterial concentration, possessing a detection range of 7.5–10 × $10^7$ CFU/mL with detection limit of 6 CFU/mL. Hence, MOFs are ideal candidates for the detection of infectious agents. Although these materials have several routine synthesis methods, their synthesis is typically time-consuming and expensive (Stock and Biswas, 2012). In biomedical applications, there is a need to use cost-effective, eco-friendly, and adjustable nanomaterials as a priority (Ahmadi et al., 2020; Parsa et al., 2018).

In order to amplify the biocompatibility of nanomaterials targeted for biomedicine as well as to avoid environmental contamination, it is pivotal to synthesize materials via green solvents (e.g., water) as well as utilizing natural raw materials (as precursors including plant extracts and natural dyes, along with employing low temperature of synthesis (Rahimnejad et al., 2021a; Rahimnejad et al., 2021b; Seidi et al., 2021). In situ and one-pot synthesis, approaches could lower production byproduct rate, which is highly desirable to meet the green chemistry criteria (Bagherzadeh et al., 2021; Rabiee et al., 2020a; Rabiee et al., 2020b). Besides, the MOFs' cytotoxicity depends on the synthesis method and their critical factors, including solvent, reaction time, temperature, stabilizer, and environmental condition (Rabiee et al., 2022; Rabiee et al., 2021g; Saeb et al., 2021a). Accordingly, altering the synthesis methods to greener techniques may diminish the cytotoxicity of MOF-based devices. In light of this, our recently developed approach, the high-gravity technique (Kiani et al., 2021; Rabiee et al., 2020c), was employed to synthesize MOF-5 and in situ growth of $CoNi_2S_4$. It should be noted that the high-gravity technique is an eco-friendly technique that usually leads to lower reaction time and temperature. Thus, the synthesized platform is greener than the other conventional approaches (Rabiee et al., 2020c).

To date, several researchers have been conducted to develop a suitable sensitizer for biosensors. Porphyrins were suitable for different materials due to their low cytotoxicity, high quantum yield, and tunable chemical structure. Porphyrins have different chemical properties based on their functionalization and metal-coordinated approaches. The rigid porphyrins can enhance nano architectures' detection limit and sensitivity (Rabiee et al., 2020d; Saeb et al., 2021b).

On the other hand, efforts have been directed towards promoting the selectivity of biosensors. For example, the $CoNi_2S_4$ nanostructures possess a unique spatial shape, and they are capable of enhancing the selectivity of

biosensors. However, $CoNi_2S_4$ nanoparticles suffer from poor biocompatibility, and one of the strategies for reducing their cytotoxicity towards normal cells is to embed them inside the porosity of MOFs. Then, natural precursors such as the bioactive coating can improve biocompatibility (Ahmadi et al., 2021; Jouyandeh et al., 2022; Maghsoudi et al., 2021).

In this work, as a proof-of-concept, a cost-effective and one-pot synthetic route was developed to fabric MOF-5 decorated with the in-situ growth $CoNi_2S_4$. Subsequently, the MOF-5/$CoNi_2S_4$ was adorned with the porphyrins $H_2$TMP. The ability of the synthesized nanocomposite to detect the recombinant SARS-CoV-2 spike antigen was investigated through an easy and reputable optical method. In addition, the treatment of HEK-293, MCF-7, HepG2, PC12, and HeLa cell lines was considered a method to investigate the potential biocompatibility and cytotoxicity of the synthesized nanomaterial. This study provides new insight into the development of green-modified nano architectures as biosensors for diagnosing SARS-CoV-2.

## 2. Materials and methods

### 2.1. One-pot synthesis of MOF-5/$CoNi_2S_4$ in assistance of high-gravity

For the first time, the MOF-5 was synthesized via a facile and high-gravity technique. Briefly, 1.5 mmol of $Zn(NO_3)_26H_2O$ and 0.5 mmol of terephthalic acid ($H_2$BDC) were mixed together and transferred to a 100 mL jar, and the mixture was dissolved via the addition of 52 mL of DMF and 1.3 mL of deionized water. In this step, the modified rotating packed bed (RPB) system was applied, which has a sealed ring and a packed rotator, and a jacket for temperature control and the necessary inlets and outlets. The RPB system was set up as described in our previous articles (Ghadiri et al., 2020; Kiani et al., 2020b). For the synthesis procedure, the solution mixture was transferred to the internal circulation space of the RPB system through the inlet. The rotation of this RPB system was adjusted with the 1400 rpm, which resulted in the high-gravity factor of 182.

The temperature of the RPB system was adjusted at 88 °C (that is more than 20 °C below the typical reaction protocols (Brozek and Dincă, 2012; Tranchemontagne et al., 2008)), and the internal space of the RPB was degassed with flowing the oxygen for 1.5 h prior to starting the system. After about 75 min, the samples were cooled down to room temperature under the gas flow of $NH_3$, and after that, the central system of RPB was degassed with the $N_2$, and $Ni(NO_3)_2.6H_2O$ (2 mmol), $Co(NO_3)_2.6H_2O$ (1 mmol) and thiourea (9 mmol) were added to the above solution, and the system runs for about 5.5 h. After that, the samples were cooled down to room temperature under the gas flow of $NH_3$, and then, the central system of RPB was degassed with the $N_2$ prior to collecting the samples.

### 2.2. Fabrication of nano biosensor for recombinant SARS-CoV-2 spike antigen assay

Determination of the possible interactions between the recombinant SARS-CoV-2 spike antigen and the synthesized nanomaterials has been conducted by incorporating the prepared $H_2$TMP (5 mg in 12 mL DMF) on the surface of the in situ synthesized nanomaterial and exposing that to different weight ratios of recombinant SARS-CoV-2 spike antigen. The procedure for one-pot synthesis of MOF-5/$CoNi_2S_4$ nanocomposites and fabrication of biosensors for recombinant SARS-CoV-2 spike antigen assay is shown in Fig. 1.

### 2.3. Cell evaluations

All of the applied nanomaterials have been exposed to ultraviolet radiations to be sterilized and washed ethanol (75%) and PBS solution for further purifications. The precise and defined cytocompatibility assessment was performed using the routine MTT (3-[4,5-dimethylthiazol-2-yl]-2,5-diphenyltetrazolium bromide) (MTT, Sigma) method at 24 and 48 h of time points.

Four cell lines of PC12 cells (ATCC CRL-1721™), HEK-293(ATCC CRL-1721™), HeLa (ATCC CCL-2), and HepG2 (ATCC HB 8065) have been applied for this study. In this regard, $1 \times 10^5$ cells per well were cultured in the presence of the synthesized nanomaterials in Dulbecco's Modified Eagle's Medium (DMEM, Gibco) containing 100 IU/mL penicillin, 100 IU/mL streptomycin (Invitrogen), and 10% fetal bovine serum (FBS; Gibco) and incubated at 37 °C at 5% $CO_2$. At each time point, 100 μL MTT solution (5 mg/mL in PBS) was added to each well. After 4 h incubation, the medium was removed, and the formazone precipitates were dissolved in dimethyl sulfoxide (DMSO; Sigma-Aldrich). The optical absorbance was measured at 570 nm using a microplate Elisa reader (ELX808, BioTek). At least three samples were averaged to calculate each time point.

### 2.4. Statistical analysis

The statistical analysis was performed using one-way analysis of variance (ANOVA), and all of the presented data means of ±SD of at least three independent sets of experiments.

## 3. Results and discussion

### 3.1. Characterizations

The FTIR and XRD spectrum results are in good agreement with the literature (Fig. 2a and b). FTIR spectrum clearly showed that the peaks at around 600–1250 $cm^{-1}$ correspond to the BDC carboxylate groups out-of-plane vibrations, as well as the characteristic peaks of the MOF-5 observed at 1410 $cm^{-1}$, 1564 $cm^{-1}$, 1510 $cm^{-1}$, and 1732 $cm^{-1}$, which correspond to the asymmetric and symmetric stretching bands of the carboxylate groups. In addition, the fingerprint absorption peaks of $CoNi_2S_4$, which are 3451 $cm^{-1}$, 1630 $cm^{-1}$, 1370 $cm^{-1}$, 901 $cm^{-1}$, and 610 $cm^{-1}$, correspond to the stretching and bending vibrations of the water compartment (OH) on the surface of the Co (Co-O-H), C-O-C vibrations, N-C = S and CS vibrations of the thiourea, respectively (Bhardwaj et al., 2020; Du et al., 2014; Jing et al., 2020; Patil et al., 2017), indicating the successful in situ and one-pot synthesis of nanocomposite along with $CoNi_2S_4$.

The XRD pattern represents the indicative peaks at $2\theta = 50.2^o$, $47.1^o$, $38.0^o$, $31.4^o$, $26.6^o$, and $16.2^o$, which is proof of the successful in situ synthesis and incorporation of $CoNi_2S_4$ in the MOF-5 structure (Li et al., 2018; Mei et al., 2014). Those peaks are in good agreement with the JCPDS 00–024-0334 (Tsukasaki et al., 2019). It should be noted that some of the $2\theta = +50^o$ have very low intensity in the XRD pattern due

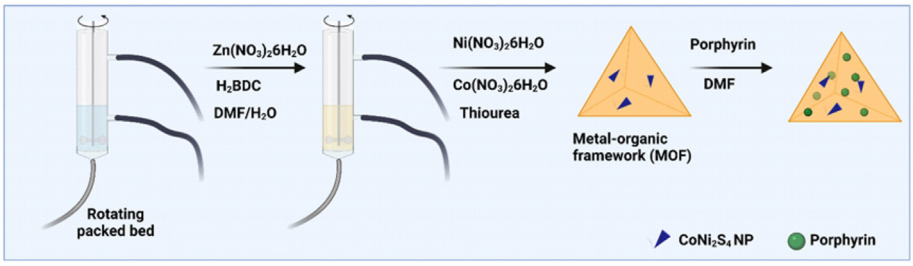


**Fig. 1.** Schematic illustration of the one-pot synthesis of MOF-5/$CoNi_2S_4$ nanocomposites and nanomaterial fabrication for recombinant SARS-CoV-2 spike antigen assay.

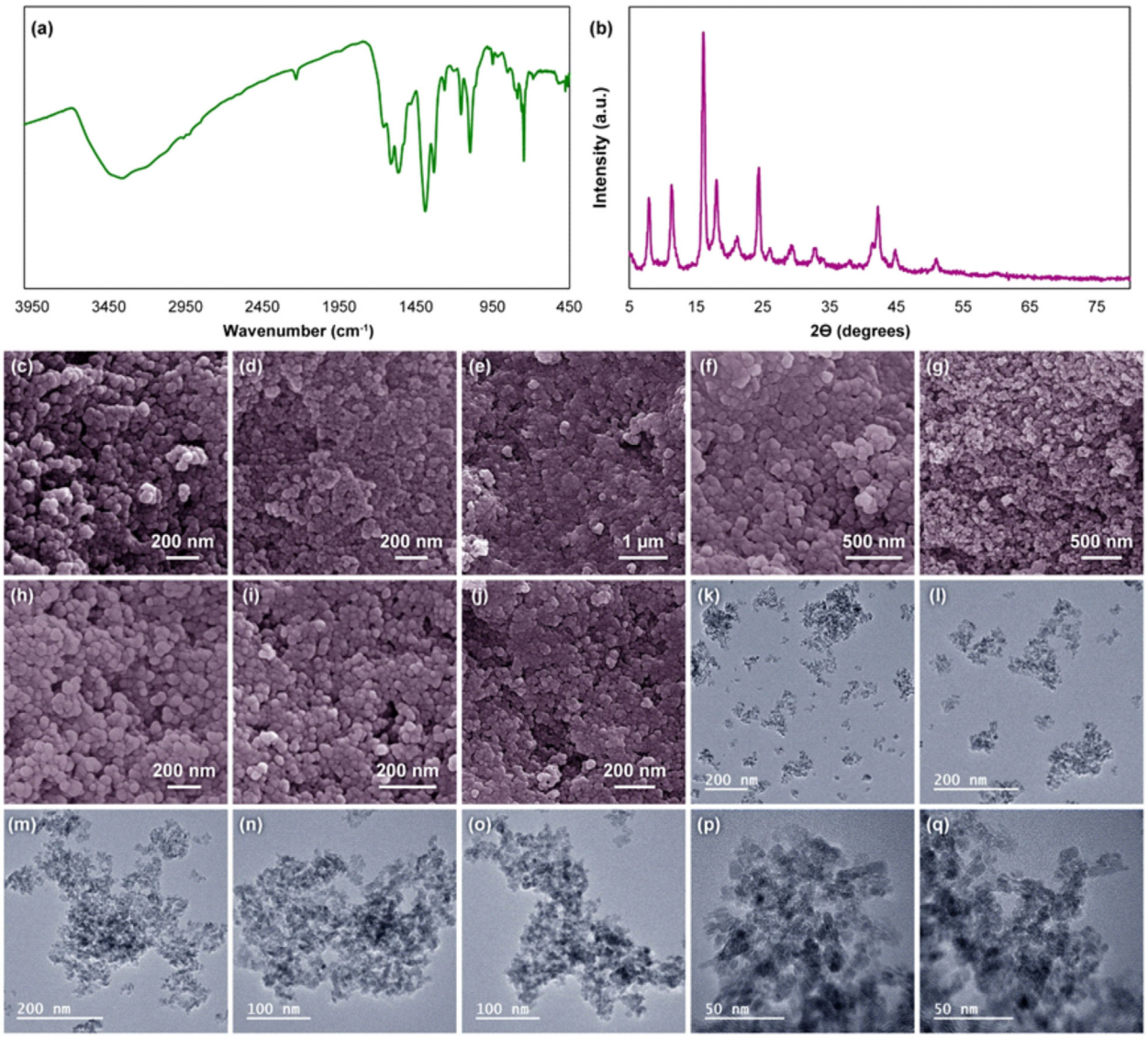


**Fig. 2.** FTIR (a), XRD (b), FESEM (c, d, e, f, g, h, i and j), and TEM (k, l, m, n, o, p and q) results of the one-pot synthesized MOF-5/$CoNi_2S_4$ in assistance of high-gravity technique.

to the presence of $CoNi_2S_4$ in the structure and matrix of MOF-5 and their interference with the X-ray diffractions. The morphology analysis was conducted with FESEM and TEM and clearly showed that the semi-cubic structure of the MOF-5 in the FESEM images (Fig. 2) and rode-like $CoNi_2S_4$ nanostructures coated on the surface of the MOF-5 in the TEM images (Fig. 2). Besides, HRTEM images of the synthesized nanocomposites (Figs. S1-S8) clearly approved the successful synthesis and the mentioned morphology of the nanostructures.

Based on the AFM results (Fig. 3; and Figs. S9, S10, and S11), different types of roughness have been observed in different spots. In Figs. 3A, B, and C, the roughness is all about the surface decorated nanoparticles in the range of the mix presence of MOF-5/$CoNi_2S_4$, 0.5 to 1.1 μm; however, in Fig. 3D, E and F, this presence dominates by mostly the $CoNi_2S_4$ species on the surface of MOF-5, in the range of 0.75 to 0.93 μm. By changing the spot of the nanostructure, based on Fig. 3G, H, and I, the roughness is more homogenous than the two other mentioned spots, 0.54 to 0.74 μm. From another perspective, Fig. 3J, K, and L showed the most homogenous roughness compared to other parts, 0.78 to near 0.80 μm.

Therefore, it could be possible to consider that the $CoNi_2S_4$ species are accumulated on different parts of the MOF-5, in some cases, on the porosity, and the other cases, on the surface of the MOF-5. Based on the literature, the high roughness usually leads to considerable aggregations on the cell walls and significant cytotoxicity (Rabiee et al., 2021a; Rabiee et al., 2021c; Rabiee et al., 2021d; Rabiee et al., 2021e; Rabiee et al., 2021f). Therefore, the minimal and controlled roughness in some spots could be able to control both the cytocompatibility and cytotoxicity.

### 3.2. Cellular experiments

Although significant efforts have been made to develop biosensors for diagnosing human diseases (Banerjee and Jaiswal, 2018), the clinical application of such devices is limited due to their safety concerns. Hence, recently much attention has been directed towards applying novel methods for the synthesis of nanostructures for diagnostic aims. The recent experiments that have synthesized MOFs for cargo delivery and detection have paid exceptional attention to these nano architectures' biocompatibility.

For instance, γ-cyclodextrin MOF crystals have been developed for pulmonary delivery of budesonide, and cell viability assay revealed high biocompatibility and safety profile of nanoparticles towards A549 cells (cell viability more than 90%) (Hu et al., 2019). Another study developed MOF-5 for drug delivery, and MTT assay was used to evaluate the safety profile of nanocarriers. Different concentrations of nanoparticles, including

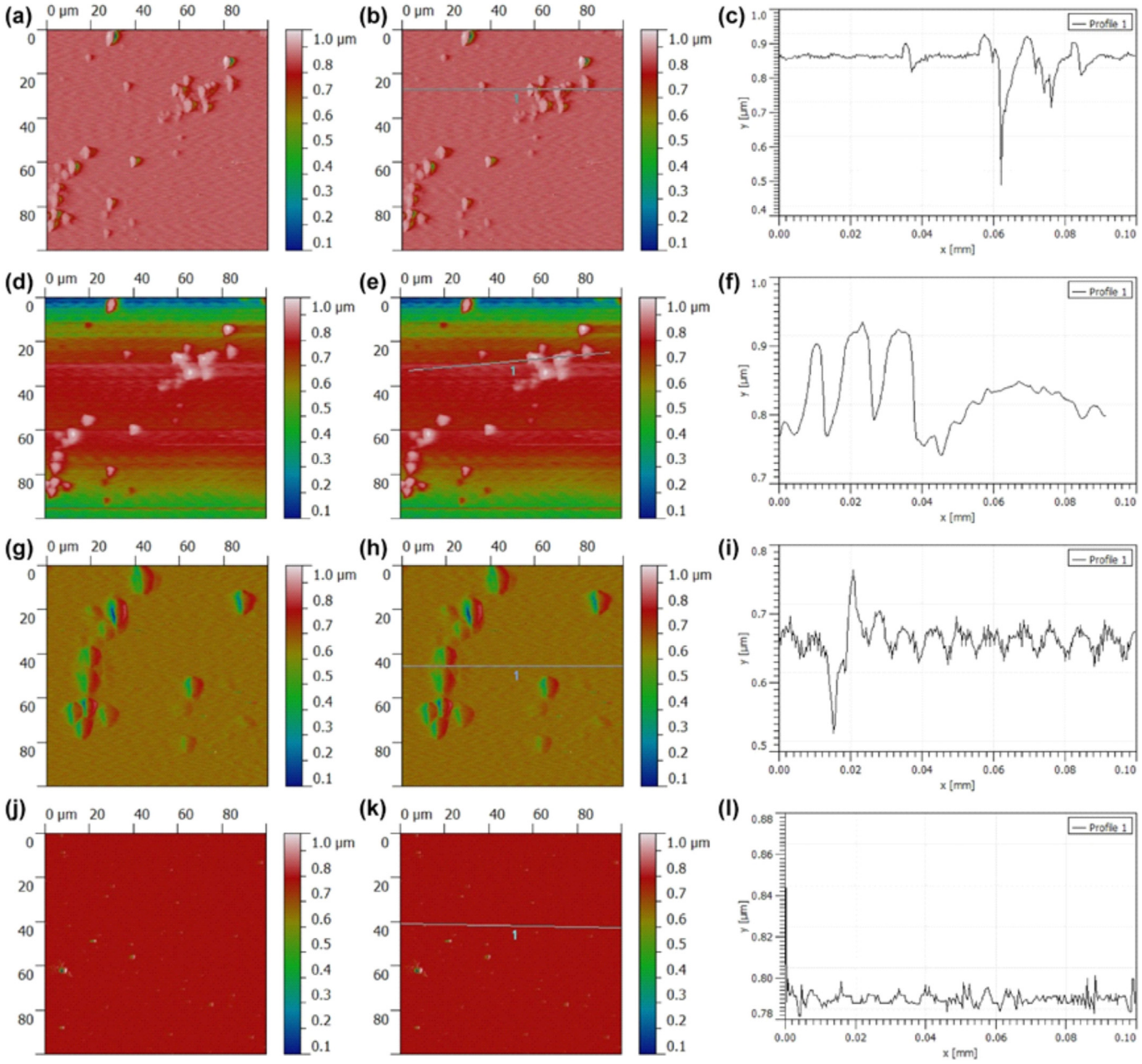


**Fig. 3.** AFM results of the one-pot synthesized MOF-5/$CoNi_2S_4$ with the assistance of the high-gravity technique from different perspectives. Normal AFM images (a, d, g, and j); roughness labeled AFM images (b, e, h, and k) and the line roughness (c, f, I, and l).

5, 10, 15, 20, and 25 μg/mL, were used, and in all cases, cell viability was more than 80–85%, showing good biocompatibility of nano architectures (Chen et al., 2019). Another experiment developed Fe-soc-MOF nanostructures for photothermal therapy, and cell viability assay (MTT) and flow cytometry revealed high biocompatibility of nanostructures, no significant decrease in viability of cells, and no death (Cai et al., 2018). We also performed MTT to investigate the biocompatibility of MOF-5. For this purpose, two kinds of normal cells, including HEK-293 (fibroblasts) and PC12 (neuron) cells, were chosen. Furthermore, like tumor cells, MCF-7 (breast cancer) and HepG2 (liver cancer) were selected to investigate toxicity.

Figs. 4 and 5 demonstrate cytotoxicity of MOF-5, high-gravity MOF-5, and high-gravity MOF-5/$CoNi_2S_4$ on HEK-293 cells, while high-gravity MOF-5 has the lowest toxicity. The high-gravity MOF-5/$CoNi_2S_4$ has better biocompatibility than normal MOF-5, but it is lower than high-gravity MOF-5. This is maybe due to the presence of $CoNi_2S_4$ in MOF-5, which has low biocompatibility. A similar is true for PC12 cells (Fig. 5). However, it is worth mentioning that after 48 h and 72 h, high-gravity MOF-5/$CoNi_2S_4$ has the lowest cytotoxicity on PC12 cells. This shows that toxicity and biocompatibility are context- and time-dependent. Figs. 6 and 7 show the toxicity of nanostructures on HeLa and HepG2 cells, respectively. In both cancer cells, high-gravity MOF-5 has the highest biocompatibility, while high-gravity MOF-5/$CoNi_2S_4$ has the lowest biocompatibility. Overall, the presence of $CoNi_2S_4$ increased the cytotoxicity that would be because of the nickel, which is highly toxic even in the ppm concentrations.

The cellular investigations represent a suitable form of cobalt and nickel-based nanomaterials with higher cellular viability than the literature. Furthermore, it should be noted that the electron transfer between the MOF-5 and CoNi2S4 could be able to increase the interactions with the rigid-porphyrin, and this leads to increasing the sensitivity of the

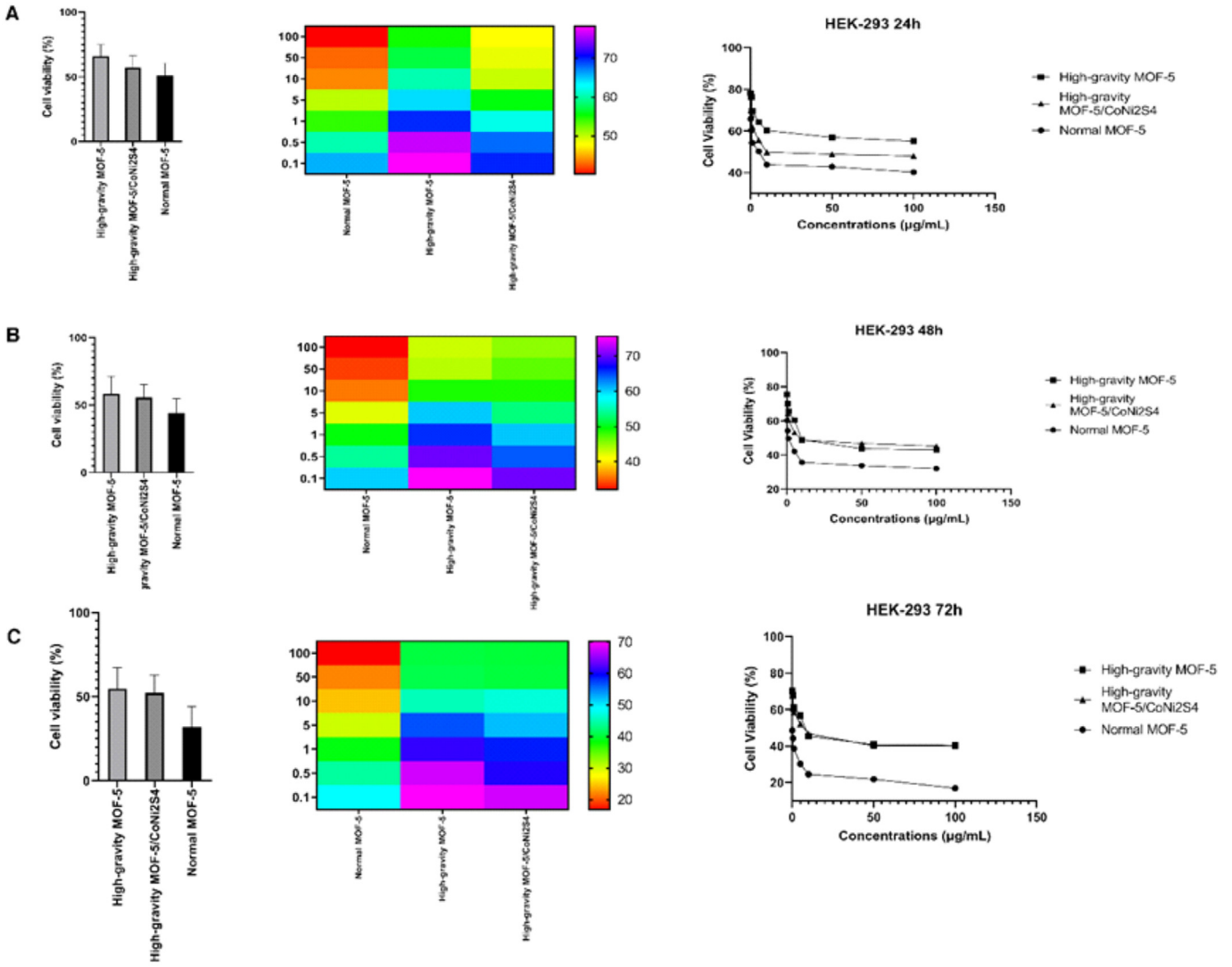


**Fig. 4.** The MTT assay of HEK-293 cells after 24 h (A), 48 h (B), and 72 h (C) of treatment. These results advocate that using the high-gravity technique enables the synthesis of nanoparticles with high biocompatibility. In addition, these nanostructures show low toxicity on HEK-293 cells as normal cells.

porphyrin to different types of analytes (Ahmadi et al., 2020; Kiani et al., 2020a; Rabiee et al., 2021b; Rauwel et al., 2020; Türkez et al., 2020).

Furthermore, the cytocompatibility and the biocompatibility potentials of the synthesized nanomaterial in the presence of the HEK-293 cell line (Fig. 8 and S12) were investigated. Based on the confocal laser microscopy (CLSM) images, after 4 h of treatment, the cellular density was not decreased, and also the 4′,6-diamidino-2-phenylindole (DAPI)-stained cells have remained intact. This phenomenon would be because of the chemical/physical changes in the environment of the synthesis method, which leads to a substantial decrease in the cytotoxicity and improves the cell-cell type interrelations between the nanostructures and the cellular microenvironments. Besides, the DAPI-stained MCF-7 cells were also screened in the presence of the synthesized nanomaterials (Fig. 8). The results showed that the cytocompatibility of the synthesized nanomaterial is in the range of optimal values and could not be able to kill/destroy the MCF-7 cells as well.

### 3.3. Biosensor analysis

Significant attempts have been made to synthesize MOF for detection, and each experiment provides a different detection limit. For instance, a recent study developed Cd-MOF/$Tb^{3+}$ ultrathin nanosheets to detect cefixime. The resulting nano architectures had better detection capacity than conventional and bulk Cd-MOF/Tb3 + sensors, and the detection limit was 16.7 nM for cefixime (Qin et al., 2021). Another experiment prepared amine-functionalized MOF nanosheets to detect hydrogen peroxide, and the detection limit was reported to be 26.9 nM (Chen et al., 2021). Furthermore, a study prepared a hybrid of MOF and quantum dots to detect riboflavin with a limit of 15 nM (Feng et al., 2021). In order to improve the capacity of MOFs in detection and increase sensitivity compared to conventional nano architectures, the synthesis method can be changed.

The ability of the synthesized nanocomposite based on the MOF-5 and $CoNi_2S_4$ towards optical detection of trace-concentrations of recombinant SARS-CoV-2 spike antigen was investigated in the presence of different concentrations of that. The results (Fig. 9) showed that the nanocomposite has considerable sensitivity towards recombinant SARS-CoV-2 spike antigen, even more than the recent studies with the same sensitizer, porphyrins (Ma et al., 2021; Mougang et al., 2021). Therefore, it could be considered that the role of the porphyrin, $H_2TMP$, in these optical biosensors is not as much as the role of the substrate. In order to be exact, the MOF-based substrate could lead to the formation of different interconnected pores and channels, and this porosity could have a significant impact on the loading/decorating with $CoNi_2S_4$ and even porphyrins. Therefore, the role of $CoNi_2S_4$ and porphyrins are dependent on the structure and morphology

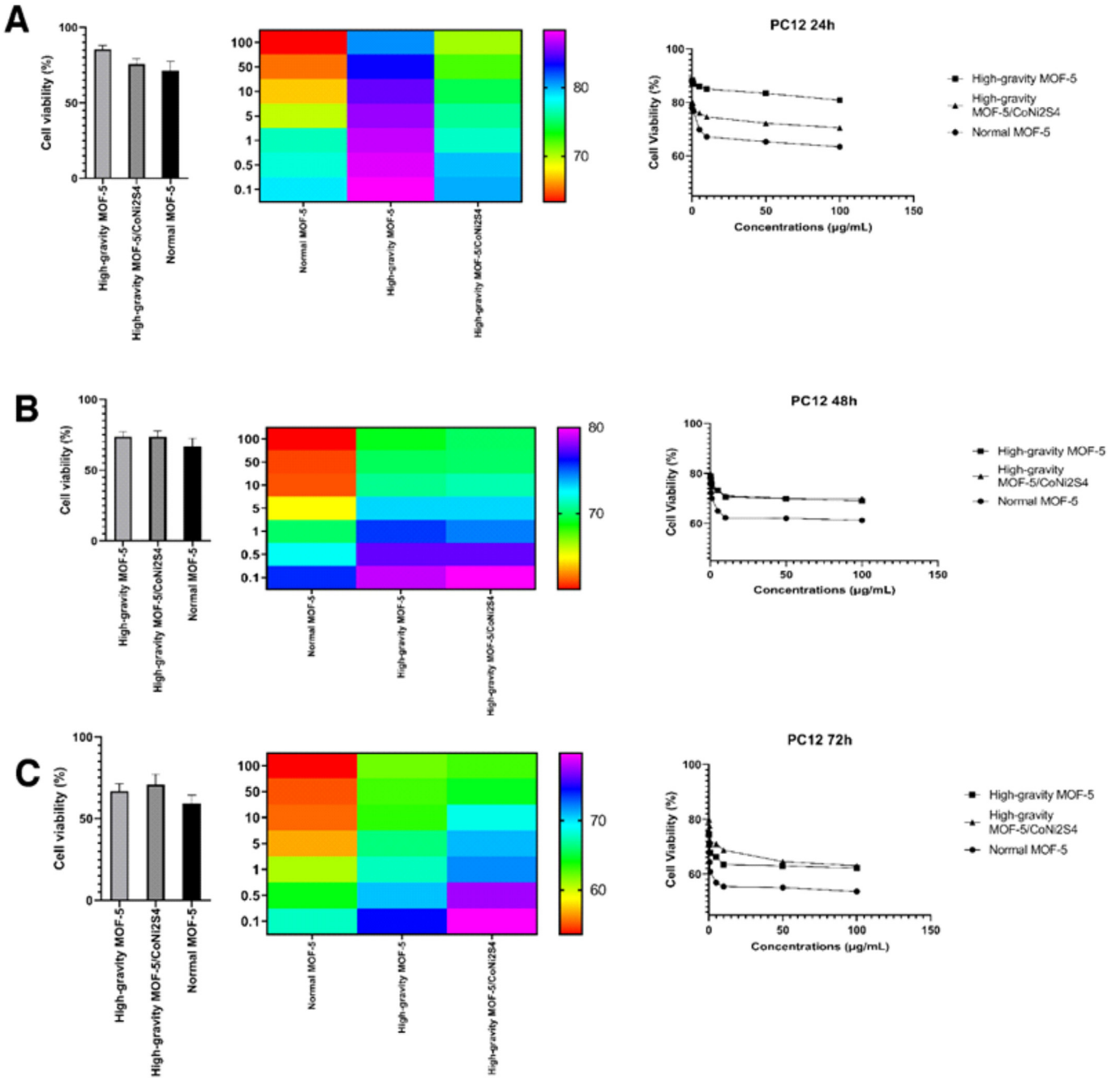


**Fig. 5.** The MTT assay on PC12 cells after 24 h (A), 48 h (B), and 72 h (C) of treatment. Cell viability decreases over time, and high-gravity MOF-5 has the highest biocompatibility within 24 h. After 48 and 72 h, biocompatibility is highest for high-gravity MOF-5/$CoNi_2S_4$ nano architectures.

of MOF. In this study, the detection limit was found to be around 5 nM, which is highly competitive with other studies.

The fluorescence quenching mechanism is related to surface physical/chemical aggregations of the recombinant SARS-CoV-2 spike antigens and tailoring the bandgap of the sensitizer. Moreover, the results were compared with the literature in Table 1. Therefore, we believe that the present method is safer, greener, more cost-effective, and easier than electrochemical sensors. In general, electrochemical biosensors have a better limit of detection even better linear range, but because of their high cost of preparation and their difficulty in use, they can be replaced with optical biosensors that are not perfect in terms of their limit of detection. Therefore, in this study, our goal was not to provide a biosensor with excellent limit detection but to reduce the cost of preparation and provide a technique to detect the coronavirus via a simple, green, and cost-effective one.

## 4. Conclusion

For the first time, MOF-5/$CoNi_2S_4$ was synthesized via a facile and one-pot method with the assistance of the high-gravity technique. The results confirmed the successful fabrication method. The morphology of the synthesized nanocomposite was investigated by FESEM and TEM, showing semi-cylindric nanostructures of the $CoNi_2S_4$ on the surface of MOF-5, with the average particle size between 25 and 80 nm for the $CoNi_2S_4$ nanoparticles. These nanoparticles were decorated with a rigid structure of porphyrins, $H_2TMP$, and the ability of the whole nanostructure, bulk, and

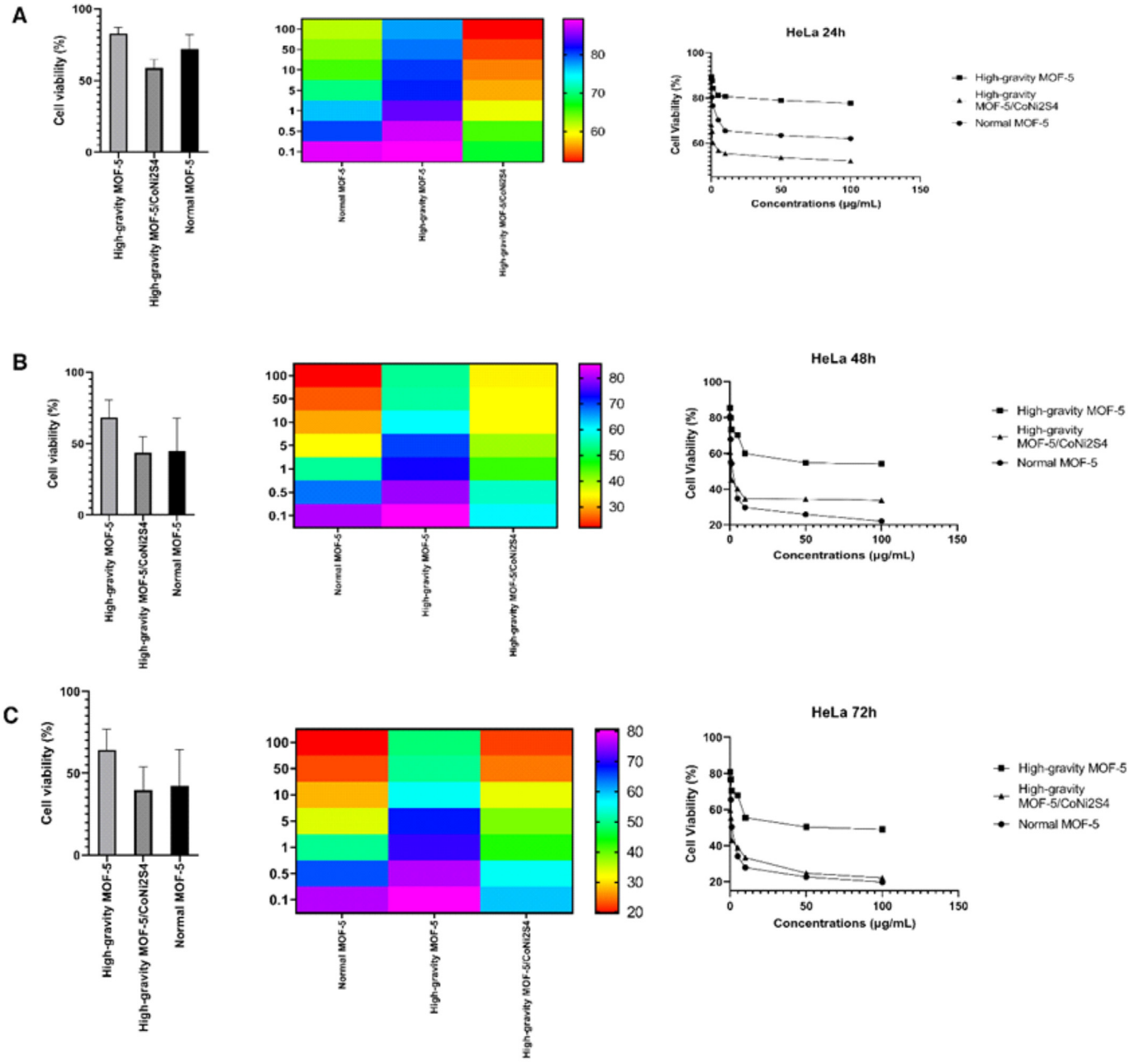


**Fig. 6.** The MTT assay of HeLa cells after 24 h (A), 48 h (B), and 72 h (C) of treatment with nanostructures. Similar to normal cells, MOF-5/$CoNi_2S_4$ nanoparticles demonstrated high biocompatibility on HeLa cells. In addition, high-gravity synthesis was responsible for reduced toxicity on HeLa cells.

crystal form, to detect the recombinant SARS-CoV-2 spike antigen was investigated by optical methods. MTT assay showed low cytotoxicity towards both HEK-293 and HeLa cell lines; the results showed more than 65% relative cell viability for both of the cell lines.

Furthermore, the cytocompatibility of the synthesized nanomaterial in the presence of HEK-293 and MCF-7 cell lines were screened by DAPI-stained cells and showed no considerable damage to the cell walls. One of the challenges in working with cytotoxic nanoparticles like $CoNi_2S_4$ is their ability to change the morphology of the cells. In this regard, the morphology of those two mentioned cell lines was screened, and the results showed no observable changes in the morphology. Therefore, we can conclude that using the inorganic-organic nanocomposite consisting of MOF-5 and porphyrins could reduce the interactions with the cell walls. The limit of detection of 5 nM was obtained, which is highly promising with a cost-effective and straightforward optical nano-bio-probe.

## Abbreviation

| | |
|---|---|
| DMEM | Dulbecco's Modified Eagle's Medium |
| COVID-19 | coronavirus disease 19 |
| CT | computed tomography |
| MOFs | metal-organic frameworks |
| RPB | rotating packed bed |
| FBS | fetal bovine serum |
| DMS | dimethyl sulfoxide |
| CLSM | confocal laser microscopy |

## CRediT authorship contribution statement

**Navid Rabiee:** Project administration, Conceptualization, Data curation, Investigation, Methodology, Software, Writing- original draft, Supervision. **Fatemeh Radmanesh:** Data curation, Investigation, Validation.

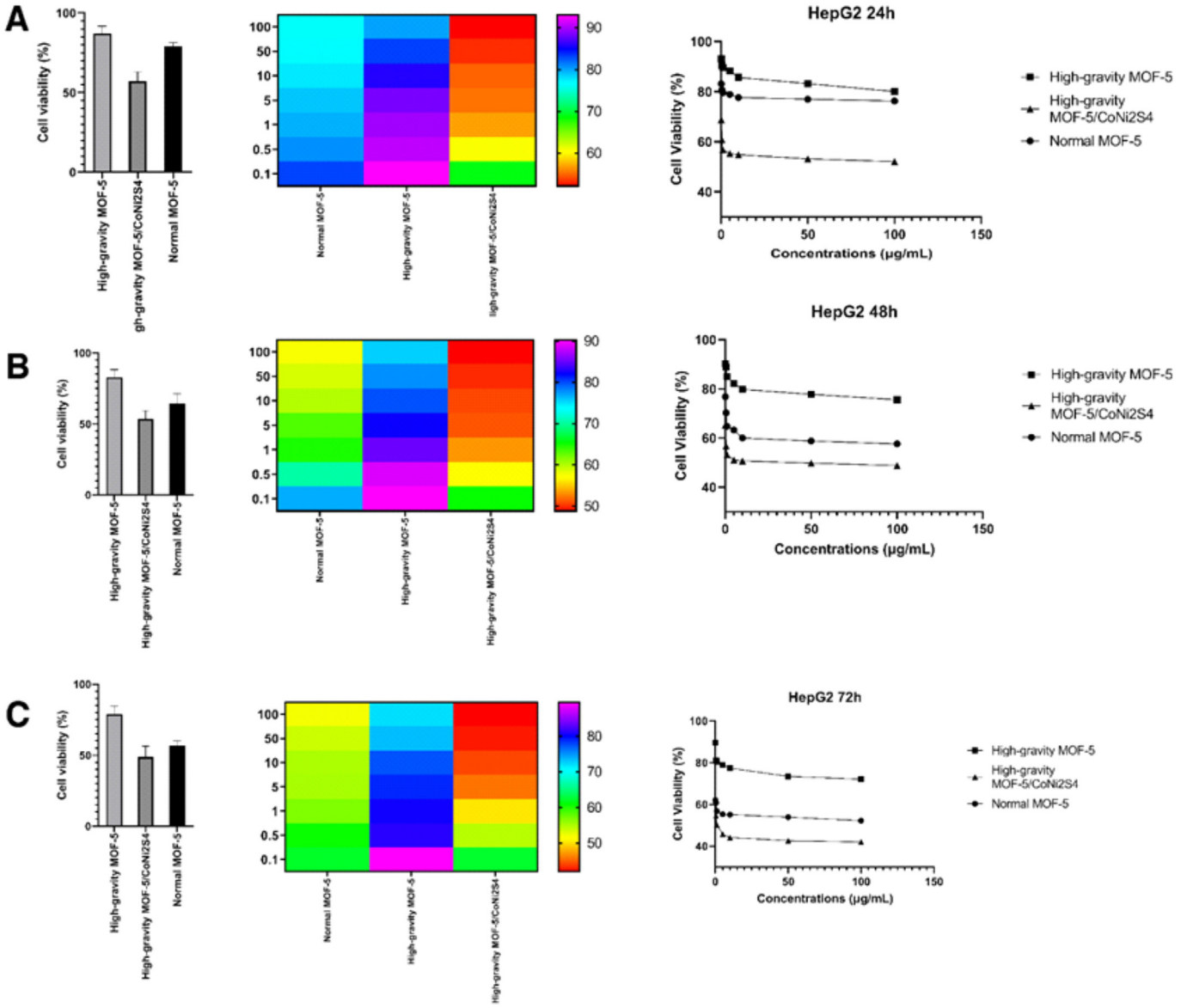


**Fig. 7.** The MTT assay on HepG2 cells after 24 h (A), 48 h (B), and 72 h (C). The highest biocompatibility is attributed to high-gravity MOF-5, while the lowest biocompatibility is related to high-gravity MOF-5/$CoNi_2S_4$.

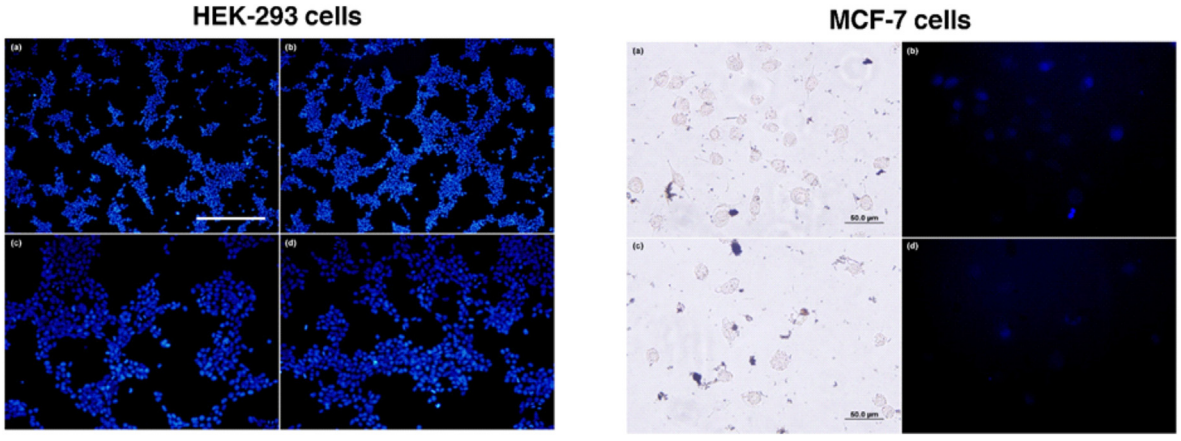


**Fig. 8.** The CLSM images of HEK-293 and MCF-7 (b) and (d) cell lines were treated with the synthesized nanomaterials. The scale bar is 50 μm (all of the panels). The CLSM images showed no morphology changes, which is another proof of the safety of the nanomaterial and in-line with the MTT results. The MCF-7 (a) and (c) are optical images confirming the biocompatibility of nanostructures.

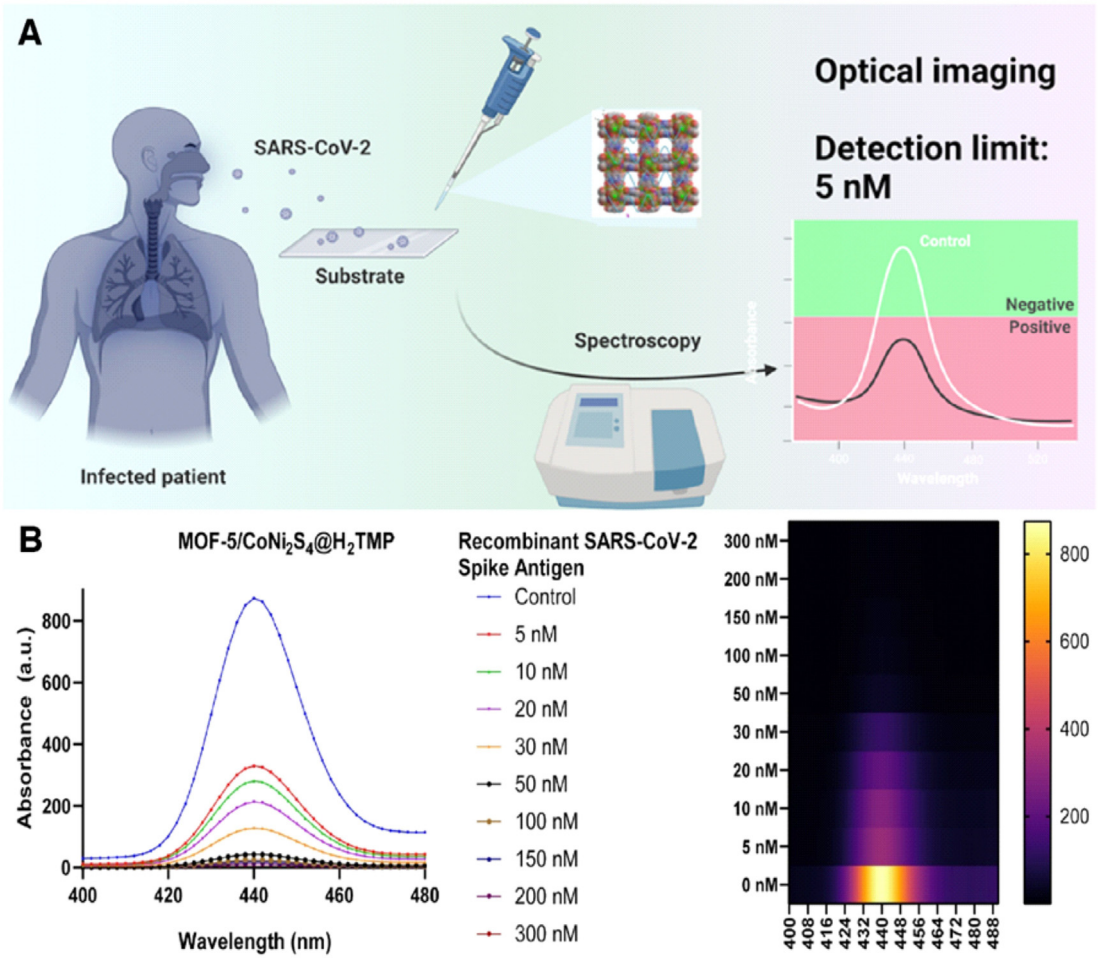


**Fig. 9.** (A) Schematic representation of MOF-5/$CoNi_2S_4$ nanostructures for optical imaging. (B) The fluorescence spectra of the optical probe in the presence of different concentrations of recombinant SARS-CoV-2 spike antigen and the heat map of the changes.

**Yousef Fatahi:** Visualization, Writing- original draft. **Sepideh Ahmadi:** Investigation, Methodology, Software. **Nikzad Abbariki:** Investigation, Methodology, Software. **Mohammad Rabiee:** Writing- original draft, Validation. **Rassoul Dinarvand:** Writing- original draft, Validation. **Amirhossein Ojaghi:** Review & editing the manuscript, Investigation. **Ebrahim Mostafavi:** Review & editing the manuscript, Validation. **Eder C. Lima:** Conceptualization, Supervision, review & editing the manuscript. **Milad Ashrafizadeh:** Writing-original draft, Methodology. **Pooyan Makvandi:** Writing-original draft, Investigation. **Mohammad Reza Saeb:** Supervision, review & editing the manuscript, Validation.

**Table 1**
A literature survey on the developed biosensors for the detection of SARS-CoV-2.

| The method and the used biosensor | Limit of detection and Limit of quantification | Notes | Reference |
|---|---|---|---|
| Optical biosensor based on AuNPs monoclonal antibody | 48 ng/mL; 50 ng/mL | Simple and rapid detection in saliva sample; dual-sensing mode exhibited; No cross-activity with other viruses | (Karakuş et al., 2021) |
| Cell-based technique based on a PDMS layer | 1 fg/mL; 10 fg/mL | Simple, rapid, and portable device | (Mavrikou et al., 2020) |
| Electrochemical immunosensor based on magnetic beads | 19 ng/mL; 30 ng/mL | High cost of preparation; affordable to be used in the clinics | (Fabiani et al., 2021) |
| Homogeneous circle-to-circle amplification real-time optomagnetic detection | 0.4 fM; 10 fM | A sub-femtomolar detection limit was achieved with a total assay time of 100 min.; The cascade amplification was performed in one-pot with real-time sensing. | (Tian et al., 2020) |
| miRNA biosensor based on localized surface plasmon resonance-enhanced | 1 pM; Not applicable | The limit of detection and specificity of the biosensor is within a diagnostically-useful range; The biosensor can quantitate specific microRNA in 1 h and can be multiplexed | (Miti et al., 2020) |
| Detection by using gold nano spikes in optofluidics | 0.5 pM; Not applicable | The sensing platform achieves the limit of detection of ~ 0.5 pM (0.08 ng/mL) and takes up to 30 min to complete the sample analysis | (Funari et al., 2020) |
| Optical biosensor based on MOF-5@$CoNi_2S_4$@$H_2$TMP | 5 nM; Not applicable | The first SARS-CoV-2 optical biosensor based on MOF-5 and CoNi2S4; investigating the role of porphyrins and porous materials in the coronavirus detection | This work |

## Declaration of competing interest

The authors declare that they have no known competing financial interests or personal relationships that could have appeared to influence the work reported in this paper.

## Acknowledgment

The authors sincerely acknowledge Dr. Mohammadreza Shokouhimehr (Seoul National University, Republic of Korea) for assistance in taking the HRTEM images. In addition, E.C. Lima thanked CNPq, CAPES, and FAPERGS for financial support and fellowships.

## Appendix A. Supplementary data

Supplementary data to this article can be found online at https://doi.org/10.1016/j.scitotenv.2022.153902.

## References

Ahmadi, S., Rabiee, N., Bagherzadeh, M., Elmi, F., Fatahi, Y., Farjadian, F., Baheiraei, N., Nasseri, B., Rabiee, M., Dastjerd, N.T., 2020. Stimulus-responsive sequential release systems for drug and gene delivery. Nano Today 34, 100914.

Ahmadi, S., Rabiee, N., Fatahi, Y., Hooshmand, S.E., Bagherzadeh, M., Rabiee, M., Jajarmi, V., Dinarvand, R., Habibzadeh, S., Saeb, M.R., 2021. Green chemistry and coronavirus. 100415.

Bagherzadeh, M., Rabiee, N., Fatahi, Y., Dinarvand, R., 2021. Zn-rich (GaN) 1–x (ZnO) x: a biomedical friend? New J. Chem. 45 (8), 4077–4089.

Banerjee, R., Jaiswal, A., 2018. Recent advances in nanoparticle-based lateral flow immunoassay as a point-of-care diagnostic tool for infectious agents and diseases. Analyst 143 (9), 1970–1996. https://doi.org/10.1039/c8an00307f.

Bhardwaj, N., Bhardwaj, S.K., Mehta, J., Kim, K.-H., Deep, A.J.A.A.M., Interfaces, 2017. MOF–bacteriophage Biosensor for Highly Sensitive and Specific Detection of Staphylococcus aureus. 9(39), pp. 33589–33598.

Bhardwaj, R.K., Jayanthi, S., Adarakatti, P.S., Sood, A., Bhattacharyya, A.J., 2020. Probing the extent of polysulfide confinement using CoNi2S4 additive inside sulfur cathode of Na/Li-sulfur rechargeable battery. ACS Appl. Mater. Interfaces.

Bhavya, B., Pathak, E., Mishra, R., 2022. Endogenous Pancreatic microRNAs differentially target the Delta, Omicron, and Wuhan SARS-CoV-2 genomes to upregulate the Diabetes-associated genes. bioRxiv.

Bidram, E., Esmaeili, Y., Amini, A., Sartorius, R., Tay, F.R., Shariati, L., Makvandi, P.J.A.B.S., Engineering, 2021. Nano-based Platforms for Diagnosis and Treatment of COVID-19: From Benchtop to Bedside.

Brozek, C.K., Dincă, M., 2012. Lattice-imposed geometry in metal-organic frameworks: lacunary Zn 4 O clusters in MOF-5 serve as tripodal chelating ligands for Ni 2+. Chem. Sci. 3 (6), 2110–2113.

Buitrago-Garcia, D., Egli-Gany, D., Counotte, M.J., Hossmann, S., Imeri, H., Ipekci, A.M., Salanti, G., Low, N.J.P.M., 2020. Occurrence and Transmission Potential of Asymptomatic and Presymptomatic SARS-CoV-2 Infections: A Living Systematic Review and Meta-analysis. 17(9), p. e1003346.

Cai, X., Liu, B., Pang, M., Lin, J., 2018. Interfacially synthesized Fe-soc-MOF nanoparticles combined with ICG for photothermal/photodynamic therapy. Dalton Trans. 47 (45), 16329–16336. https://doi.org/10.1039/c8dt02941e.

Chen, G., Luo, J., Cai, M., Qin, L., Wang, Y., Gao, L., Huang, P., Yu, Y., Ding, Y., Dong, X., Yin, X., Ni, J., 2019. Investigation of metal-organic framework-5 (MOF-5) as an antitumor drug oridonin sustained release carrier. Molecules 24 (18). https://doi.org/10.3390/molecules24183369.

Chen, G., Wu, D., Guo, W., Cao, Y., Huang, D., Wang, H., Wang, T., Zhang, X., Chen, H., Yu, H., Zhang, X., Zhang, M., Wu, S., Song, J., Chen, T., Han, M., Li, S., Luo, X., Zhao, J., Ning, Q., 2020. Clinical and immunological features of severe and moderate coronavirus disease 2019. J. Clin. Invest. 130 (5), 2620–2629.

Chen, J., Xu, Y., Xu, F., Zhang, Q., Li, S., Lu, X., 2021. Detection of hydrogen peroxide and glucose with a novel fluorescent probe by the enzymatic reaction of amino-functionalized MOF nanosheets. Anal. Methods 13 (37), 4228–4237. https://doi.org/10.1039/d1ay00190f.

Chung, M., Bernheim, A., Mei, X., Zhang, N., Huang, M., Zeng, X., Cui, J., Xu, W., Yang, Y., Fayad, Z.A.J.R., 2020. CT Imaging Features of 2019 Novel Coronavirus (2019-nCoV). 295(1), pp. 202–207.

Drobysh, M., Ramanaviciene, A., Viter, R., Chen, C.-F., Samukaite-Bubniene, U., Ratautaite, V., Ramanavicius, A., 2022. Biosensors for the determination of SARS-CoV-2 virus and diagnosis of COVID-19 infection. Int. J. Mol. Sci. 23 (2), 666.

Drobysh, M., Ramanaviciene, A., Viter, R., Ramanavicius, A., 2021. Affinity sensors for the diagnosis of COVID-19. Micromachines 12 (4), 390.

Dronina, J., Samukaite-Bubniene, U., Ramanavicius, A., 2021. Advances and insights in the diagnosis of viral infections. J. Nanobiotechnol. 19 (1), 1–23.

Du, W., Wang, Z., Zhu, Z., Hu, S., Zhu, X., Shi, Y., Pang, H., Qian, X., 2014. Facile synthesis and superior electrochemical performances of CoNi 2 S 4/graphene nanocomposite suitable for supercapacitor electrodes. J. Mater. Chem. A 2 (25), 9613–9619.

Fabiani, L., Saroglia, M., Galatà, G., De Santis, R., Fillo, S., Luca, V., Faggioni, G., D'Amore, N., Regalbuto, E., Salvatori, P., 2021. Magnetic beads combined with carbon black-based screen-printed electrodes for COVID-19: a reliable and miniaturized electrochemical immuno-sensor for SARS-CoV-2 detection in saliva. Biosens. Bioelectron. 171, 112686.

Feng, S., Pei, F., Wu, Y., Lv, J., Hao, Q., Yang, T., Tong, Z., Lei, W., 2021. A ratiometric fluorescent sensor based on g-CNQDs@Zn-MOF for the sensitive detection of riboflavin via FRET. Spectrochim. Acta A Mol. Biomol. Spectrosc. 246, 119004. https://doi.org/10.1016/j.saa.2020.119004.

Funari, R., Chu, K.-Y., Shen, A.Q., 2020. Detection of antibodies against SARS-CoV-2 spike protein by gold nano spikes in an opto-microfluidic chip. Biosens. Bioelectron. 169, 112578.

Furukawa, H., Cordova, K.E., O'Keeffe, M., Yaghi, O.M.J.S., 2013. The Chemistry and Applications of Metal-organic Frameworks. 341(6149).

Ghadiri, A.M., Rabiee, N., Bagherzadeh, M., Kiani, M., Fatahi, Y., Di Bartolomeo, A., Dinarvand, R., Webster, T.J., 2020. Green synthesis of CuO-and Cu2O-NPs in assistance with high-gravity: the flowering of nanobiotechnology. Nanotechnology 31 (42), 425101.

Hornuss, D., Lange, B., Schröter, N., Rieg, S., Kern, W.V., Wagner, D., 2020. Anosmia in COVID-19 patients. Clin. Microbiol. Infect. 26 (10), 1426–1427. https://doi.org/10.1016/j.cmi.2020.05.017.

Hu, W.C., Pang, J., Biswas, S., Wang, K., Wang, C., Xia, X.H., 2021. Ultrasensitive detection of bacteria using a 2D MOF nanozyme-amplified electrochemical detector. Anal. Chem. 93 (24), 8544–8552. https://doi.org/10.1021/acs.analchem.1c01261.

Hu, X., Wang, C., Wang, L., Liu, Z., Wu, L., Zhang, G., Yu, L., Ren, X., York, P., Sun, L., Zhang, J., Li, H., 2019. Nanoporous CD-MOF particles with uniform and inhalable size for pulmonary delivery of budesonide. Int. J. Pharm. 564, 153–161. https://doi.org/10.1016/j.ijpharm.2019.04.030.

Huang, C., Wang, Y., Li, X., Ren, L., Zhao, J., Hu, Y., Zhang, L., Fan, G., Xu, J., Gu, X.J.T.L., 2020. Clinical Features of Patients Infected With 2019 Novel Coronavirus in Wuhan, China. 395(10223), pp. 497–506.

Iravani, S., 2020. Nano-and biosensors for the detection of SARS-CoV-2: challenges and opportunities. Mater. Adv. 1 (9), 3092–3103.

Jing, C., Guo, X., Xia, L., Chen, Y., Wang, X., Liu, X., Dong, B., Dong, F., Li, S., Zhang, Y., 2020. Morphologically confined hybridization of tiny CoNi2S4 nanosheets into S, P co-doped graphene leading to enhanced pseudocapacitance and rate capability. Chem. Eng. J. 379, 122305.

Jouyandeh, M., Tavakoli, O., Sarkhanpour, R., Sajadi, S.M., Zarrintaj, P., Rabiee, N., Akhavan, O., Lima, E.C., Saeb, M.R., 2022. Green products from herbal medicine wastes by subcritical water treatment. J. Hazard. Mater. 424, 127294.

Karakuş, E., Erdemir, E., Demirbilek, N., Liv, L., 2021. Colorimetric and electrochemical detection of SARS-CoV-2 spike antigen with a gold nanoparticle-based biosensor. Anal. Chim. Acta 1182, 338939.

Kiani, M., Bagherzadeh, M., Meghdadi, S., Rabiee, N., Abbasi, A., Schenk-Joß, K., Tahriri, M., Tayebi, L., Webster, T.J., 2020a. Development of a novel carboxamide-based off–on switch fluorescence sensor: Hg 2+, Zn 2+ and Cd 2+. New J. Chem. 44 (27), 11841–11852.

Kiani, M., Rabiee, N., Bagherzadeh, M., Ghadiri, A.M., Fatahi, Y., Dinarvand, R., Webster, T.J., 2020b. High-gravity assisted green synthesis of palladium nanoparticles: the flowering of nanomedicine. Nanomedicine 102297.

Kiani, M., Rabiee, N., Bagherzadeh, M., Ghadiri, A.M., Fatahi, Y., Dinarvand, R., Webster, T.J., 2021. Improved green biosynthesis of chitosan decorated Ag-and Co3O4-nanoparticles: a relationship between surface morphology, photocatalytic, and biomedical applications. Nanomedicine 32, 102331.

Kumar, N., Shetti, N.P., Jagannath, S., Aminabhavi, T.M., 2022. Electrochemical sensors for the detection of SARS-CoV-2 virus. Chem. Eng. J. 430, 132966.

Li, Z., Zhao, D., Xu, C., Ning, J., Zhong, Y., Zhang, Z., Wang, Y., Hu, Y., 2018. Reduced CoNi2S4 nanosheets with enhanced conductivity for high-performance supercapacitors. Electrochim. Acta 278, 33–41.

Lu, Q., Su, T., Shang, Z., Jin, D., Shu, Y., Xu, Q., Hu, X., 2021. Flexible paper-based ni-MOF composite/AuNPs/CNTs film electrode for HIV DNA detection. Biosens. Bioelectron. 184, 113229. https://doi.org/10.1016/j.bios.2021.113229.

Ma, J., Wang, W., Li, Y., Lu, Z., Tan, X., Han, H., 2021. Novel porphyrin Zr metal-organic framework (PCN-224)-based ultrastable electrochemiluminescence system for PEDV sensing. Anal. Chem. 93 (4), 2090–2096.

Maddali, H., Miles, C.E., Kohn, J., O'Carroll, D.M.J.C., 2021. Optical Biosensors for Virus Detection: Prospects for SARS-CoV-2/COVID-19. 22(7), p. 1176.

Maghsoudi, S., Taghavi Shahraki, B., Rabiee, N., Fatahi, Y., Bagherzadeh, M., Dinarvand, R., Ahmadi, S., Rabiee, M., Tahriri, M., Hamblin, M.R., 2021. The colorful world of carotenoids: a profound insight on therapeutics and recent trends in nano delivery systems. Crit. Rev. Food Sci. Nutr. 1–40.

Mavrikou, S., Moschopoulou, G., Tsekouras, V., Kintzios, S., 2020. Development of a portable, ultra-rapid, and ultra-sensitive cell-based biosensor for the direct detection of the SARS-CoV-2 S1 spike protein antigen. Sensors 20 (11), 3121.

Mei, L., Yang, T., Xu, C., Zhang, M., Chen, L., Li, Q., Wang, T., 2014. Hierarchical mushroom-like CoNi2S4 arrays as a novel electrode material for supercapacitors. Nano Energy 3, 36–45.

Miti, A., Thamm, S., Müller, P., Csáki, A., Fritzsche, W., Zuccheri, G., 2020. A miRNA biosensor based on localized surface plasmon resonance-enhanced by surface-bound hybridization chain reaction. Biosens. Bioelectron. 167, 112465.

Mougang, Y.K., Di Zazzo, L., Minieri, M., Capuano, R., Catini, A., Legramante, J.M., Paolesse, R., Bernardini, S., Di Natale, C., 2021. Sensor array and gas chromatographic detection of the blood serum volatolomic signature of COVID-19. Iscience 24 (8), 102851.

Parsa, S.F., Vafajoo, A., Rostami, A., Salarian, R., Rabiee, M., Rabiee, N., Rabiee, G., Tahriri, M., Yadegari, A., Vashaee, D., 2018. Early diagnosis of disease using microbead array technology: a review. Anal. Chim. Acta 1032, 1–17.

Patil, S., Kim, J., Lee, D., 2017. Self-assembled Ni3S2//CoNi2S4 nanoarrays for ultra-high-performance supercapacitor. Chem. Eng. J. 322, 498–509.
Plikusiene, I., Maciulis, V., Ramanaviciene, A., Balevicius, Z., Buzavaite-Verteliene, E., Ciplys, E., Slibinskas, R., Simanavicius, M., Zvirbliene, A., Ramanavicius, A., 2021. Evaluation of kinetics and thermodynamics of interaction between immobilized SARS-CoV-2 nucleoprotein and specific antibodies by total internal reflection ellipsometry. J. Colloid Interface Sci. 594, 195–203.
Qin, G., Wang, J., Li, L., Yuan, F., Zha, Q., Bai, W., Ni, Y., 2021. Highly water-stable cd-MOF/Tb(3+) ultrathin fluorescence nanosheets for ultrasensitive and selective detection of cefixime. Talanta 221, 121421. https://doi.org/10.1016/j.talanta.2020.121421.
Quijia, C.R, Alves, R.C., Hanck-Silva, G., Galvão Frem, R.C., Arroyos, G., Chorilli, M., 2021. Metal-organic frameworks for diagnosis and therapy of infectious diseases. Crit Rev. Microbiol. 1–36.
Rabiee, N., Bagherzadeh, M., Ghadiri, A.M., Fatahi, Y., Aldhaher, A., Makvandi, P., Dinarvand, R., Jouyandeh, M., Saeb, M.R., Mozafari, M., 2021. Turning toxic nanomaterials into a safe and bioactive nanocarrier for co-delivery of DOX/pCRISPR. ACS Appl. Bio Mater. 4 (6), 5336–5351.
Rabiee, N., Bagherzadeh, M., Ghadiri, A.M., Fatahi, Y., Baheiraei, N., Safarkhani, M., Aldhaher, A., Dinarvand, R., 2021b. Bio-multifunctional noncovalent porphyrin functionalized carbon-based nanocomposite. Sci. Rep. 11 (1), 1–15.
Rabiee, N., Bagherzadeh, M., Ghadiri, A.M., Kiani, M., Ahmadi, S., Aldhaher, A., Varma, R.S., Webster, T.J., 2020a. High-gravity-assisted green synthesis of NiO-NPs anchored on the surface of biodegradable nanobeads with potential biomedical applications. J. Biomed. Nanotechnol. 16 (4), 520–530.
Rabiee, N., Bagherzadeh, M., Ghadiri, A.M., Kiani, M., Aldhaher, A., Ramakrishna, S., Tahriri, M., Tayebi, L., Webster, T.J., 2020b. Green synthesis of ZnO NPs via Salvia hispanica: evaluation of potential antioxidant, antibacterial, mammalian cell viability, H1N1 influenza virus inhibition, and photocatalytic activities. J. Biomed. Nanotechnol. 16 (4), 456–466.
Rabiee, N., Bagherzadeh, M., Ghadiri, A.M., Kiani, M., Fatahi, Y., Tavakolizadeh, M., Pourjavadi, A., Jouyandeh, M., Saeb, M.R., Mozafari, M., 2021c. Multifunctional 3D hierarchical bioactive green carbon-based nanocomposites. ACS Sustain. Chem. Eng. 9 (26), 8706–8720.
Rabiee, N., Bagherzadeh, M., Heidarian Haris, M., Ghadiri, A.M., Matloubi Moghaddam, F., Fatahi, Y., Dinarvand, R., Jarahiyan, A., Ahmadi, S., Shokouhimehr, M., 2021d. Polymer-coated NH2-UiO-66 for the codelivery of DOX/pCRISPR. ACS Appl. Mater. Interfaces 13 (9), 10796–10811.
Rabiee, N., Bagherzadeh, M., Jouyandeh, M., Zarrintaj, P., Saeb, M.R., Mozafari, M., Shokouhimehr, M., Varma, R.S., 2021e. Natural polymers decorated MOF-MXene nanocarriers for co-delivery of doxorubicin/pCRISPR. ACS Appl. Bio Mater. 4 (6), 5106–5121.
Rabiee, N., Bagherzadeh, M., Kiani, M., Ghadiri, A.M., Zhang, K., Jin, Z., Ramakrishna, S., Shokouhimehr, M., 2020c. High gravity-assisted green synthesis of ZnO nanoparticles via Allium ursinum: conjoining nanochemistry to neuroscience. Nano Express 1 (2), 020025.
Rabiee, N., Fatahi, Y., Asadnia, M., Daneshgar, H., Kiani, M., Ghadiri, A.M., Atarod, M., Mashhadzadeh, A.H., Akhavan, O., Bagherzadeh, M., 2022. Green porous benzamide-like nanomembranes for hazardous cations detection, separation, and concentration adjustment. J. Hazard. Mater. 423, 127130.
Rabiee, N., Khatami, M., Jamalipour Soufi, G., Fatahi, Y., Iravani, S., Varma, R.S., 2021. Diatoms with invaluable applications in nanotechnology, biotechnology, and biomedicine: recent advances. ACS Biomater. Sci. Eng. 7 (7), 3053–3068.
Rabiee, N., Rabiee, M., Sojdeh, S., Fatahi, Y., Dinarvand, R., Safarkhani, M., Ahmadi, S., Daneshgar, H., Radmanesh, F., Maghsoudi, S., 2021g. Porphyrin molecules decorated on metal-organic frameworks for multi-functional biomedical applications. Biomolecules 11 (11), 1714.
Rabiee, N., Yaraki, M.T., Garakani, S.M., Garakani, S.M., Ahmadi, S., Lajevardi, A., Bagherzadeh, M., Rabiee, M., Tayebi, L., Tahriri, M., 2020d. Recent advances in porphyrin-based nanocomposites for effective targeted imaging and therapy. Biomaterials 232, 119707.
Rahimnejad, M., Nasrollahi Boroujeni, N., Jahangiri, S., Rabiee, N., Rabiee, M., Makvandi, P., Akhavan, O., Varma, R.S., 2021a. Prevascularized micro-/nano-sized spheroid/bead aggregates for vascular tissue engineering. Nano-Micro Lett. 13 (1), 1–24.
Rahimnejad, M., Rabiee, N., Ahmadi, S., Jahangiri, S., Sajadi, S.M., Akhavan, O., Saeb, M.R., Kwon, W., Kim, M., Hahn, S.K., 2021. Emerging phospholipid nanobiomaterials for biomedical applications to lab-on-a-chip, drug delivery, and cellular engineering. ACS Appl. Bio Mater. 4 (12), 8110–8128.
Rauwel, E., Al-Arag, S., Salehi, H., Amorim, C.O., Cuisinier, F., Guha, M., Rosario, M.S., Rauwel, P., 2020. Assessing cobalt metal nanoparticles uptake by cancer cells using live Raman spectroscopy. Int. J. Nanomedicine 15, 7051–7062.
Saeb, M.R., Rabiee, N., Mozafari, M., Mostafavi, E., 2021a. Metal-organic frameworks-based nanomaterials for drug delivery. Materials 14 (13), 3652.
Saeb, M.R., Rabiee, N., Seidi, F., Far, B.F., Bagherzadeh, M., Lima, E.C., Rabiee, M., 2021b. Green CoNi2S4/porphyrin decorated carbon-based nanocomposites for genetic materials detection. Journal of Bioresources and Bioproducts.
Seidi, F., Yazdi, M.K., Jouyandeh, M., Habibzadeh, S., Munir, M.T., Vahabi, H., Bagheri, B., Rabiee, N., Zarrintaj, P., Saeb, M.R., 2021. Crystalline polysaccharides: a review. Carbohydr. Polym. 118624.
Shetti, N.P., Mishra, A., Bukkitgar, S.D., Basu, S., Narang, J., Raghava Reddy, K., Aminabhavi, T.M., 2021. Conventional and nanotechnology-based sensing methods for SARS coronavirus (2019-nCoV). ACS Appl. Biomater. 4 (2), 1178–1190.
Srivastava, M., Srivastava, N., Mishra, P.K., Malhotra, B.D., 2021. Prospects of nanomaterials-enabled biosensors for COVID-19 detection. Sci. Total Environ. 754, 142363.
Stock, N., Biswas, S., 2012. Synthesis of metal-organic frameworks (MOFs): routes to various MOF topologies, morphologies, and composites. Chem. Rev. 112 (2), 933–969.
Suleman, S., Shukla, S.K., Malhotra, N., Bukkitgar, S.D., Shetti, N.P., Pilloton, R., Narang, J., Tan, Y.N., Aminabhavi, T.M., 2021. Point of care detection of COVID-19: advancement in biosensing and diagnostic methods. Chem. Eng. J. 414, 128759.
Takashita, E., Kinoshita, N., Yamayoshi, S., Sakai-Tagawa, Y., Fujisaki, S., Ito, M., Iwatsuki-Horimoto, K., Chiba, S., Halfmann, P., Nagai, H., 2022. Efficacy of antibodies and antiviral drugs against Covid-19 omicron variant. N. Engl. J. Med.
Tian, B., Gao, F., Fock, J., Dufva, M., Hansen, M.F., 2020. Homogeneous circle-to-circle amplification for real-time opto-magnetic detection of SARS-CoV-2 RdRp coding sequence. Biosens. Bioelectron. 165, 112356.
Tranchemontagne, D.J., Hunt, J.R., Yaghi, O.M., 2008. Room temperature synthesis of metal-organic frameworks: MOF-5, MOF-74, MOF-177, MOF-199, and IRMOF-0. Tetrahedron 64 (36), 8553–8557.
Tsukasaki, H., Uchiyama, T., Yamamoto, K., Mori, S., Uchimoto, Y., Kowada, H., Hayashi, A., Tatsumisago, M., 2019. Exothermal mechanisms in the charged LiNi1/3Mn1/3Co1/3O2 electrode layers for sulfide-based all-solid-state lithium batteries. J. Power Sources 434, 226714.
Türkez, H., Arslan, M.E., Sönmez, E., Tatar, A., Geyikoğlu, F., Açikyildiz, M., Mardinoğlu, A., 2020. Safety assessments of nickel boride nanoparticles on the human pulmonary alveolar cells by using cell viability and gene expression analyses. Biol. Trace Elem. Res. 1–10.
Xi, H., Juhas, M., Zhang, Y., 2020. G-quadruplex-based biosensor: a potential tool for SARS-CoV-2 detection. Biosens. Bioelectron. 167, 112494.
Xian, S., Lin, Y., Wang, H., Li, J.J.S., 2021. Calcium-based Metal-organic Frameworks and Their Potential Applications. 17(22).
Yüce, M., Filiztekin, E., Özkaya, K.G.J.B., Bioelectronics, 2021. COVID-19 Diagnosis—A Review of current methods. 172.
Zhou, F., Yu, T., Du, R., Fan, G., Liu, Y., Liu, Z., Xiang, J., Wang, Y., Song, B., Gu, X.J.T.L., 2020. Clinical Course and Risk Factors for Mortality of Adult Inpatients With COVID-19 in Wuhan, China: A Retrospective Cohort Study. 395(10229), pp. 1054–1062.